Powder Technology 269 (2015) 85–92

Contents lists available at ScienceDirect

Powder Technology

journal homepage: www.elsevier.com/locate/powtec

Nanoscale dispersion crystal bundles of palygorskite by associated modification with phytic acid and high-pressure homogenization for enhanced colloidal properties

Wenbo Wang [a,b], Fangfang Wang [a], Yuru Kang [a,b], Aiqin Wang [a,b,*]

[a] Center of Xuyi Palygorskite Applied Technology, Lanzhou Institute of Chemical Physics, Chinese Academy of Sciences, Lanzhou 730000, China
[b] Key Laboratory for Palygorskite Science and Applied Technology of Jiangsu Province, Huaiyin Institute of Technology, Huai'an 223003, China

ARTICLE INFO

Article history:
Received 25 June 2014
Received in revised form 1 September 2014
Accepted 4 September 2014
Available online 16 September 2014

Keywords:
Palygorskite
Nanoscale dispersion
Phytic acid
High-pressure homogenization
Colloidal properties

ABSTRACT

The nanoscale dispersion of rod-like crystal bundles or aggregates of natural palygorskite (PAL) is not only significant in practical application but is also a challenge. In this paper, phytic acid (PA) was introduced during high-pressure homogenization (HPH) process to simultaneously disperse PAL crystal bundles and restrain the re-aggregation of the dispersed nanorods. SEM, TEM, XRD, FTIR and N_2 adsorption–desorption analyses confirmed that the crystal bundles or aggregates of PAL were highly disaggregated and dispersed to individual nanorod with no disruption to the aspect ratio of rods after being homogenized at 30 MPa, and PA molecules are favorable to dispersion and restrain the re-aggregation of nanorods. The nanoscale dispersion of PAL rods increased the BET specific surface area and Zeta potentials, and effectively improved the colloidal properties. The colloidal viscosity of modified PAL was sharply increased by 110.4% (from 1728 mPa·s to 3636 mPa·s) at the optimal dosage of PA (0.1 wt.%) and the homogenization pressure of 30 MPa, and the suspension stability was clearly enhanced by 71%. This simple disaggregation process provides a new industrial approach to produce nanoscale PAL and extend its application in modern industry.

1. Introduction

Over the past decades, clay minerals as the materials of "greening 21st century material world" have been extensively concerned by virtue of their excellent properties and eco-friendly advantages [1–3]. Palygorskite (PAL) is a naturally available Mg-rich silicate mineral with nanorod-like crystal morphology and theoretical formula of $(Al_2Mg_2)Si_8O_{20}(OH)_2(OH_2)_4 \cdot 4H_2O$ [4]. The intrinsic microstructure of PAL endows it with the features of one-dimensional nanomaterials, and so PAL has found potential applications in many fields such as nanocomposites [5–7], catalyst supporters [8–10], crystalline film [11], adsorbents [12,13], colloidal agents [14,15] and pigment [16].

The performance of the materials derived from PAL is highly dependent on the dispersion scale of PAL nanorods [17–19]. However, the rods in natural PAL existed as bundles or "woodpile-like" aggregates because the strong hydrogen bonding and van der Waals interactions existed among rods [20]. These bulk bundles or aggregates are hardly to be dispersed into nanoscale rods by a common treatment method, and so raw PAL is only a precursor of nanomaterials, instead of a real nanomaterial. In that case, the colloidal, adsorption and reinforcing properties of natural PAL are extremely limited, and the derived materials hardly reach a satisfactory performance. Therefore, to disaggregate the crystal bundles of PAL and disperse them into nanoscale becomes the key to develop high-performance PAL-based materials.

Generally, the effective dispersion of PAL rods could be achieved by two processes: (i) using moderate mechanical treatment to take apart the crystal bundles [21]; (ii) introducing chemicals to adjust the surface character and restrain the re-aggregation of dispersed nanorods [22]. Thus far, many methods (i.e., extrusion, high-speed shearing, ultrasound, freezing and grinding) have been used to disaggregate the crystal bundles. However, these methods are subject to two contradictory problems: the disaggregation efficiency is not enough at lower shearing strength, but the excessive mechanical action may break the nanorods and decrease the aspect ratio. From the aggregation state of nanorods in natural PAL [20], it can be noticed that the aggregates or crystal bundles can be disaggregated when the external force can overcome the hydrogen-bonding or van der Waals forces existed among rods. However, in the methods described above, the imposed mechanical forces (i.e., squeezing, shearing, rub) mainly act on the rigid PAL rods, and so they have larger contribution to break rods than to disaggregate them. Furthermore, many of these methods are not suitable for large-scale industrial production.

* Corresponding author at: Center of Xuyi Palygorskite Applied Technology, Lanzhou Institute of Chemical Physics, Chinese Academy of Sciences, Lanzhou 730000, China. Tel.: +86 931 4968118; fax: +86 931 8277088.
E-mail address: aqwang@licp.cas.cn (A. Wang).

http://dx.doi.org/10.1016/j.powtec.2014.09.015
0032-5910/

Different from the conventional mechanical treatment methods, high-pressure homogenization (HPH) is a technology designed on the basis of the "Bernoulli principle", and is used for large-scale industrial refinement and dispersion [23]. In the process of homogenization, the dispersion liquids firstly pass through a pressure-adjustable homogenization valve, and the "cavitation effect" was generated due to the sudden release of pressure. The mechanical forces generated from "cavitation effect" mainly act on the gaps among the crystal bundles, and mildly "burst through" the closely intertwined nanorods. So, the crystal bundles can be disaggregated effectively without disrupting the inherent aspect ratio of nanorods [24]. In addition, the dispersants or modifiers can be easily introduced in the process of high-pressure homogenization to realize the simultaneous disaggregation of crystal bundles and the surface modification by a one-step process [22,25]. This is very significant to the large-scale industrial production.

After disaggregation, the highly dispersed nanorods may be re-aggregated during drying due to the higher surface energy of free-standing nanorods, and so moderate modifier is required to restrain the re-aggregation process. Phytic acid (PA) is a saturated cyclic acid with six $-H_2PO_3$ groups (Scheme 1), and is the principal storage form of phosphorus in many plant tissues, especially in bran and seeds [26]. PA is an innoxious, biocompatible and environment friendly organic molecule, and is usually used as corrosion resistant inhibitor of metal materials for the paint or pigment [27]. Besides, PA can interact with the silicate (SiO_2) nanoparticles (with 7.94% of P loading) to form a new material with excellent functional properties [28], and it exhibits a stronger infinity with silicates. It was expected that PA can be attached on the surface of PAL nanorod to adjust its surface properties, decreasing the re-aggregation of nanorods during drying. In addition, it may contribute to alter the self-assembly and "face-to-edge" association capability of PAL nanorods in aqueous solution to improve the colloidal properties. However, there are no researches on the combination of PA with HPH process to improve the dispersion or other performance up to now.

In order to effectively disaggregate crystal bundles of PAL, disperse them into nanoscale rods and improve its colloidal properties, in this paper, natural PAL was modified with PA under high-pressure homogenization to obtain nanoscale PAL. It was expected that the "physical" homogenization action may disaggregate the crystal bundle, and the "chemical" modification with PA may restrain the re-aggregation of PAL nanorods. The effect of nanoscale dispersion treatment on the structure and physico-chemical properties was investigated by Fourier transform infrared spectroscopy (FTIR), X-ray diffraction (XRD), scanning electronic microscopy (SEM), BET specific surface area, and Zeta potential analyses, and the colloidal viscosity, stability and rheological properties were systematically evaluated.

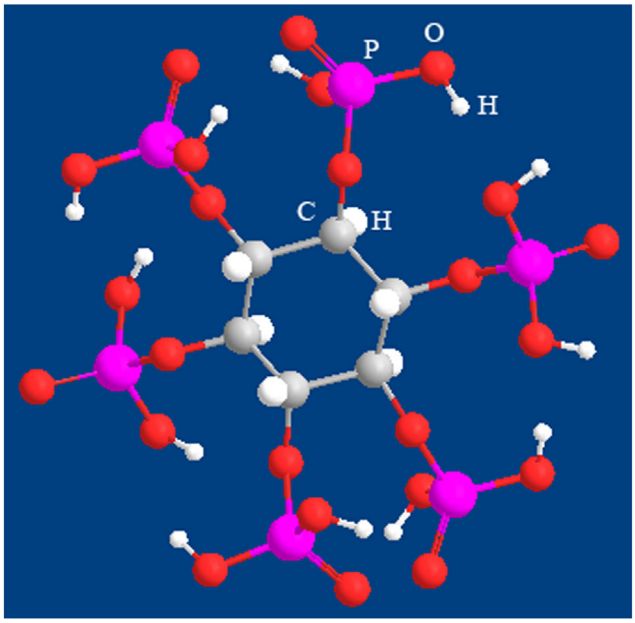

Scheme 1. Molecular structure of phytic acid.

2. Experimental

2.1. Materials

PAL clay mineral was obtained from Guanshan Mine (Anhui, China), and was three-rolled for one time before use. The main chemical composition is Al_2O_3 (10.318%), MgO (14.474%), CaO (0.694%), SiO_2 (69.264%), K_2O (0.985%), and Fe_2O_3 (5.023%). PA (biochemical reagents, BR) was purchased from Sinopharm Chemical Reagent Co., Ltd (Shanghai, China). All aqueous solution was prepared with deionized water.

2.2. Dispersion and modification of PAL

Natural PAL was simultaneously dispersed and modified by introducing PA in the HPH process. Typically, PAL was dispersed in the solution of PA (0.1 wt.%) at the solid/liquid ratio of 7/100 under continuous mechanical stirring (800 rpm, 4 h), and then filtered through a 300-mesh sieve to remove the undesirable quartz. The filtered suspension was divided into six equal parts, and then homogenized under different pressures (0 MPa, 10 MPa, 20 MPa, 30 MPa, 40 MPa and 50 MPa) using the high-pressure homogenizer (GYB-3004, Shanghai Donghua High Pressure Homogenizer Factory, Shanghai, China). Finally, the solid product was separated by centrifugation at 4500 rpm, dried at 105 °C for 4 h, ground, and passed through a 200-mesh screen for use. The PA-modified PAL samples under different pressures were marked as pPAL-0, pPAL-10, pPAL-20, pPAL-30, pPAL-40 and pPAL-50, and the PAL sample that is only homogenized at 30 MPa (without adding PA) was marked as PAL-30.

2.3. Measurement of rotation viscosity

The homogeneous dispersion for viscosity test was prepared as the following procedure: 7.0 g of PAL samples was dispersed in 93 mL of deionized water by a high-speed stirring at 11 000 rpm for 20 min. Then, the rotary viscosity of the suspension at different shear times was measured on a ZNN-D6 rotational viscosimeter (Qingdao Camera Factory, China) at 30 rpm, using spindle 3#.

2.4. Measurement of colloidal stability

The colloidal stability of the suspension was evaluated using the conventional sedimentation method in a graduated cylinder. Generally, 2.0 g of PAL sample was dispersed in 120 mL of deionized water, and then high-speed stirring at 11 000 rpm for 10 min to form a uniform dispersion. The dispersion was transferred to a 100 mL graduated cylinder, and it was allowed to stand undisturbed for a certain time. The sedimentation volume was read directly from the graduated cylinder at a set time interval.

2.5. Measurement of rheological property

Shear rheological properties were measured on an Anton Paar Physica MCR301 Rheometer at 25 °C. For steady shear measurements, the shear rate ranged from 0.1 to 200 1/s. A cone-plate with water bath was used for all measurements. The concentration of the PAL suspension for measurement is 7.0 wt.% (mass fraction).

2.6. Characterizations

The morphologies of samples were observed using a field emission scanning electron microscope (FE-SEM, JSM-6701F, JEOL, Ltd) after coating with gold film. TEM image was taken using a JEM-1200 EX/S transmission electron microscope (TEM) (JEOL, Tokyo, Japan). The XRD patterns were collected on an X'Pert PRO diffractometer equipped with a Cu Kα radiation source (40 kV, 40 mA) from 3 to 70° with a step interval of about 0.167°. The FTIR spectra were recorded on a Thermo Nicolet NEXUS TM spectrophotometer in the range of 4000–400 cm^{-1} using a KBr platelet. The specific surface area was measured on an ASAP 2010 analyzer (Micromeritics, USA) at 77 K by the N_2 adsorption–desorption isotherms. All the samples were degassed at 90 °C for 10 h to remove moisture. The specific surface area (S_{BET}) was calculated by the BET equation. The total pore volume (V_{total}) was obtained from the volume of liquid N_2 held at the relative pressure $P/P_0 = 0.95$. The micropore volume (V_{micro}) was estimated by the *t*-plot method.

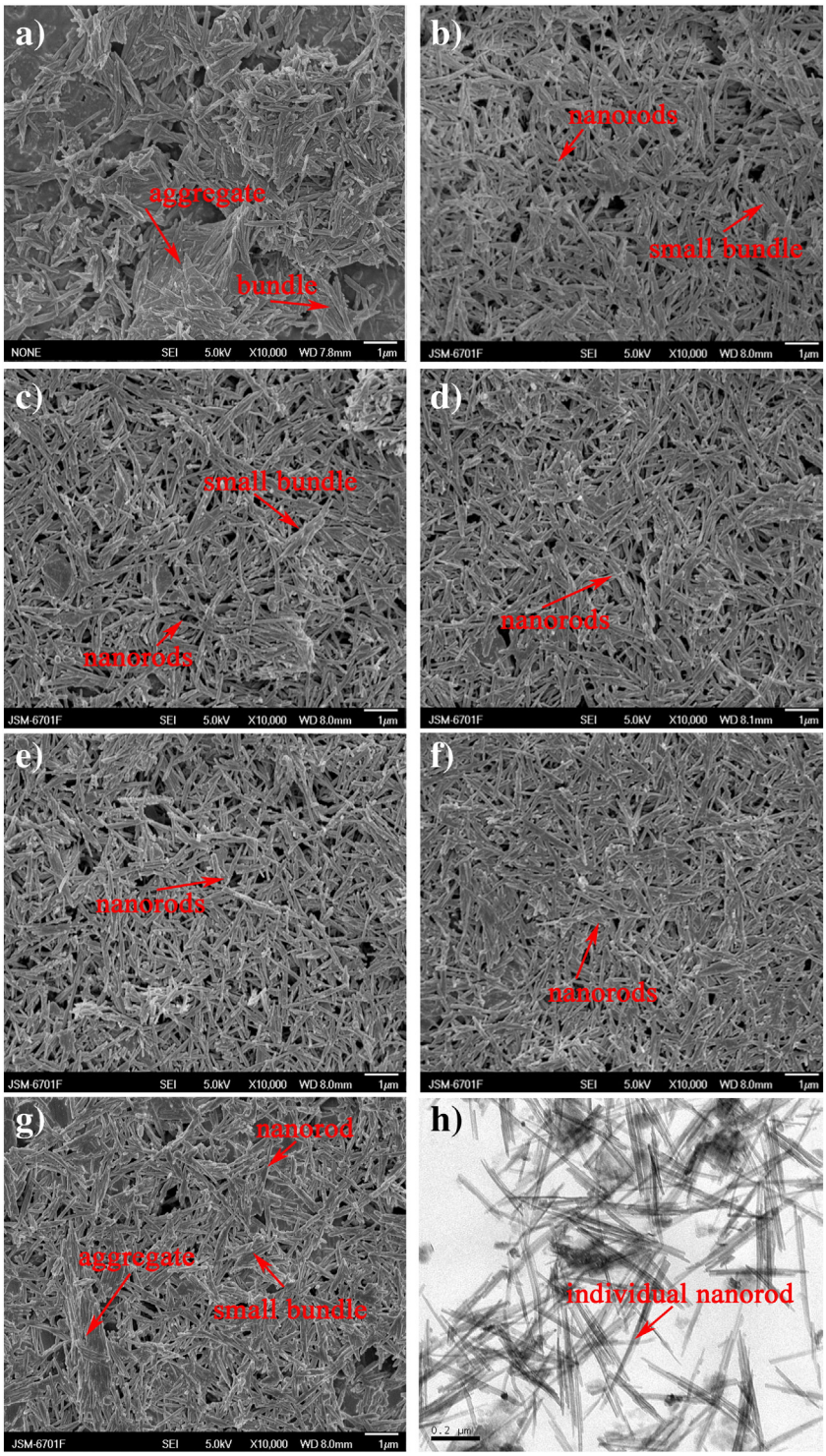

Fig. 1. SEM images of (a) pPAL-0, (b) pPAL-10, (c) pPAL-20, (d) pPAL-30, (e) pPAL-40, (f) pPAL-50 and (g) PAL-30 samples; TEM image of (h) pPAL-30.

3. Results and discussion

3.1. Nanoscale dispersion of PAL bundles

The SEM images of PA-modified PAL under different homogenization pressures are shown in Fig. 1. Many crystal bundles and aggregates can be observed in pPAL-0 sample (without homogenization), which indicates that the simple rolling pretreatment and weak mechanical stirring is not enough to disintegrate the crystal bundles of PAL (Fig. 1a). After being homogenized at 10 MPa and 20 MPa, the crystal bundles and aggregates reduced, the dispersion degree of nanorods increased, and numerous individual nanorods were observed (Fig. 1b, c). This reveals that the crystal bundles were dissociated after homogenization, even at a relatively lower pressure. With increasing the pressure to 30 MPa and 40 MPa, the dispersion degree of PAL nanorods was further increased, and the bundles were almost dispersed to nanoscale (Fig. 1d, e). Whereas, the length of nanorod has no obvious change, indicating that the HPH process can fully dissociate the crystal bundles of PAL at 30 and 40 MPa with no damage to rod crystal [24]. When the pressure was increased to 50 MPa, the length of rods was slightly decreased in comparison with the others, indicating that the exorbitant pressure may damage the rod crystal.

It can also be observed from Fig. 1(g, h) that the crystal bundles have not been effectively dispersed as individual nanorods after only homogenization (without PA) at 30 MPa and 40 MPa, indicating that the introduction of PA not only is favorable to the dispersion of nanorods, but also restrains the re-aggregation of dispersed nanorods (Scheme 2). The PA molecules with fix $-H_2PO_3$ groups may interact with the PAL nanorods. For one thing, the degree of dissociation of the acid groups could influence the aggregation via the electrostatic repulsion between phytate units; for another, the phytate units could be attached to surface metal cations of PAL via a coordinative arrangement, which may increase the steric hindrance and contact distance among nanorods and then restrain their re-aggregation.

Fig. 2 shows the XRD diffractograms of PA-modified PAL under different homogenization pressures. The (110) diffraction peaks of the pPAL homogenized at 0 MPa, 10 MPa, 20 MPa, 30 MPa, 40 MPa and 50 MPa appeared at $2\theta = 8.39°$ ($d = 1.0530$ nm), $2\theta = 8.38°$ ($d = 1.0542$ nm), $2\theta = 8.34°$ ($d = 1.0593$ nm), $2\theta = 8.34°$ ($d = 1.0593$ nm), $2\theta = 8.35°$ ($d = 1.0580$ nm) and $2\theta = 8.33°$ ($d = 1.0605$ nm), respectively [29,30]. This reveals that the (110) crystal planes of PAL have minor changes after homogenization. The interplanar spacing of (110) plane was slightly increased with increasing the pressures, and then tends to a constant value. The diffraction peaks of (110), (200), (130), (040) and (240) crystal planes of PAL have no clear change, even treated at the highest pressure (50 MPa). This implies that high-pressure action may affect the microenvironment around the tetrahedron and octahedron, but has no obvious impact on the skeleton structure of PAL crystal, which is consistent with the SEM results. As described previously, ultrasound treatment [31] or grinding treatment [32] may destroy the crystal structure of PAL. This difference further confirms that HPH technology is superior to the other mechanical treatment methods [24].

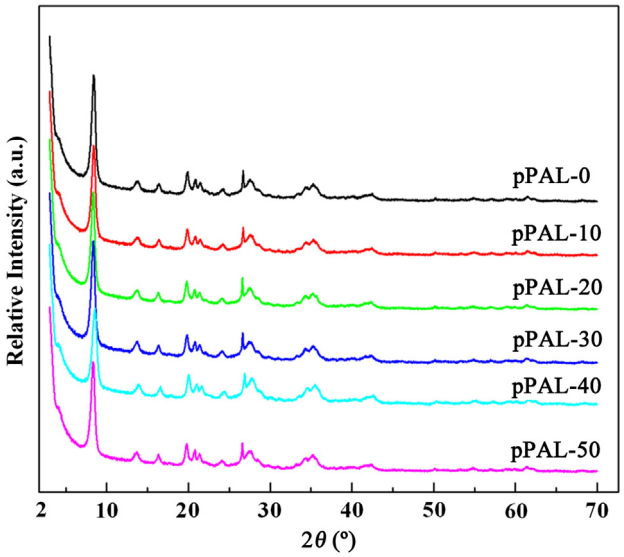

Fig. 2. XRD diffractograms of PAL modified under different homogenization pressures.

Fig. 3 shows the FTIR spectra of PA-modified PAL samples. The absorbance bands of PAL at 3615 cm^{-1}, 3581 cm^{-1}, 3551 cm^{-1} and 3524 cm^{-1} can be assigned to the O–H stretching vibration of Al_2O–H groups, the O–H stretching vibration of (Al,Fe) O–H groups, the stretching vibration of bond water OH_2, and the stretching vibration of adsorbed and zeolite water, respectively [33,34]. The bands at 1655 cm^{-1}, 1198 cm^{-1}, 982 cm^{-1} and 649 cm^{-1} are ascribed to the overlapping band of H–O–H bending vibration of adsorbed and zeolite water molecules, the stretching vibration of the Si–O–Si group connected two reverse SiO_4 tetrahedrons, the symmetric stretching vibration of Si–O–Mg and the stretching vibration of H_2O–Mg–H_2O (adsorbed water and zeolite water), respectively. These absorbance bands have no obvious changes after homogenization treatment. This indicates that the crystal structure of PAL is not destroyed during homogenization process [34], which can fit well with the SEM and XRD results.

Besides the nanorod-like crystals, the nanoporous structure of PAL is also an important physicochemical index that may greatly affect its application in many areas. The BET specific surface area (S_{BET}) of PAL is mainly dependent on the dispersion degree of nanorods and the distribution of modifiers on the surface. Generally, the S_{BET} may

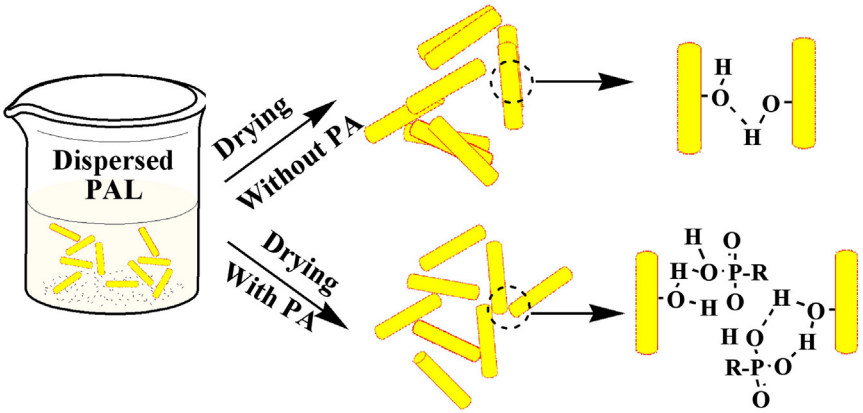

Scheme 2. The effect of PA on restraining the re-aggregation of dispersed nanorods.

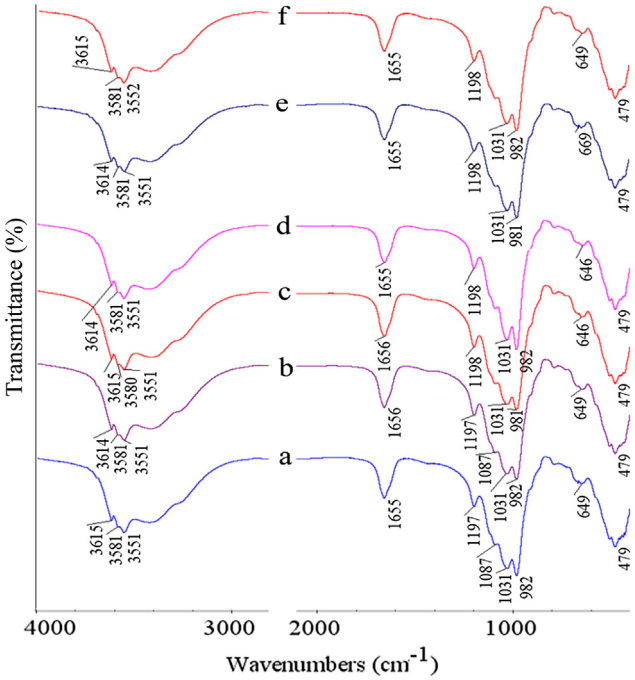

Fig. 3. FTIR spectra of (a) pPAL-0, (b) pPAL-10, (c) pPAL-20, (d) pPAL-30, (e) pPAL-40 and (f) pPAL-50.

decrease after modifying with organic molecules because they may enter the pore or coat on the surface of PAL to block the pore or tunnel [35,36]. The decrease of S_{BET} was observed in most of the surfactant-dispersed clay minerals [37], which is adverse to the practical application of clay in many cases.

The modification of PAL with PA can be confirmed by the change of P_2O_5 content (determined with the method described in Ref. [38]). The P_2O_5 content for pPAL-0 is 36.69 ppm, but it increased to 38.3 ppm (pPAL-10), 42.1 ppm (pPAL-20), 45.8 ppm (pPAL-30), 46.3 ppm (pPAL-40) and 46.8 ppm (pPAL-50) after homogenization. This indicates that the PA molecules existed on the surface of PAL, and the HPH process contributes to the attachment of PA. Despite the existence of PA molecules on PAL, it deserves to be pointed out that the modification of PAL with PA and HPH process may enhance the S_{BET}. As shown in Table 1, the S_{BET} of APT-30 is 211.12 m^2/g, but the S_{BET} of pAPT-30 can reach 231.5 m^2/g, indicating that the introduction of PA is favorable to increase the S_{BET} of PAL, instead of decreasing it. This may be due to the better dispersion and weak re-aggregation of PAL nanorods after adding PA (Scheme 2).

The HPH process has more obvious influence on the pore parameter. With increasing the homogenization pressures: (i) the specific surface area (S_{BET}) was firstly increased, reaching the maximum value (231.5 m^2/g) at 30 MPa, and then decreased; (ii) the external surface area (S_{ext}) was increased after homogenization, but the homogenization pressures have no obvious influence on S_{ext}; (iii) the micropore specific surface area (S_{micro}) was increased after being homogenized at 20, 30 and 40 MPa, but decreased at 50 MPa; (iv) the pore size (PZ) was greatly increased with increasing the homogenization pressure, and the PAL sample homogenized at 50 MPa gives the maximum PZ of 9.9216 nm; (v) the pore volume (V_{total}) was firstly increased and then decreased. The changes of pore parameters with homogenization pressure are mainly due to the disaggregation of the crystal bundles or aggregates of PAL. After being dispersed as nanoscale (see Fig. 1), more pores, especially the micropores, were uncovered and the S_{micro} has relatively greater contribution to the S_{BET}. The V_{micro} and V_{total} reached the maximum after being homogenized at 30 MPa. This indicates that more micropores were released by the "cavitation effect" generated from the HPH process, while the pores were not damaged. The dispersion of PAL by HPH process induced obvious increase of PZ in contrast to the un-homogenized sample, and the maximum PZ (9.9216 nm) was reached after being homogenized at 50 MPa due to the breakage of partial nanorods and the loss of the micropore [31]. These results also indicate that the PA molecules do not enter into the pore of PAL, and are only attached on the surface of PAL nanorods.

Table 1
BET parameters of PA-modified PAL under different homogenization pressures.

Samples	Different homogenization pressures					
	pPAL-0	pPAL-10	pPAL-20	pPAL-30	pPAL-40	pPAL-50
$S_{BET}/m^2/g$	213.65	217.36	219.09	231.50	225.95	215.57
$S_{micro}/m^2/g$	84.53	84.60	87.61	98.95	92.88	83.72
$S_{ext}/m^2/g$	129.12	132.76	131.48	132.55	133.08	131.84
$V_{micro}/cm^3/g$	0.0447	0.0443	0.0459	0.0518	0.0487	0.0438
$V_{total}/cm^3/g$	0.4820	0.4982	0.5414	0.5691	0.5447	0.5347
PZ/nm	9.0246	9.1691	9.8848	9.8328	9.6432	9.9216

After PAL crystal bundles were dispersed as nanoscale rods, the Zeta potentials were also changed. As shown in Fig. 4, the Zeta potential of un-homogenized sample is −15.67 mV. After homogenization at different pressures, the Zeta potentials were increased to −16.07 mV (for 10 MPa), −16.08 (for 20 MPa), −16.27 mV (for 30 MPa), −16.3 mV (for 40 MPa), and −16.27 mV (for 50 MPa). The Zeta potential of pPAL-40 reached the minimum. The change of Zeta potentials is mainly due to, (i) the full dissociation of crystal bundles as highly dispersed PAL nanorods may uncover more surface groups and –Si–O^- bonds to increase the potential on the surface of PAL [15,39]; (ii) more PA molecules can attach on the surface of PAL after homogenization treatment due to the efficient dispersion of crystal bundles, which give rise to the increase of surface negative charges.

3.2. Colloidal properties

The nanoscale dispersion contributes to improve the colloidal properties, and in turn the improvement of colloidal properties may also reflect the dispersion of nanorods. As shown in Fig. 5, the viscosity of the dispersion of PAL decreased with prolonging the shear time, which presents an obvious shear-thinning thixotropic behavior that is essential for the application of clay in many areas including coating, daily chemicals, and paint. The rotary viscosity of the PAL dispersion was initially increased and then decreased with increasing the homogenization pressure, and the PAL homogenized at 30 MPa gives the optimal viscosity of 3636 mPa·s (Fig. 5a). This viscosity value can meet the practical usage requirement of colloidal PAL in fine chemical industries. By comparison with the colloidal system based on the PAL modified with other methods (or modifiers), this viscosity is the optimum.

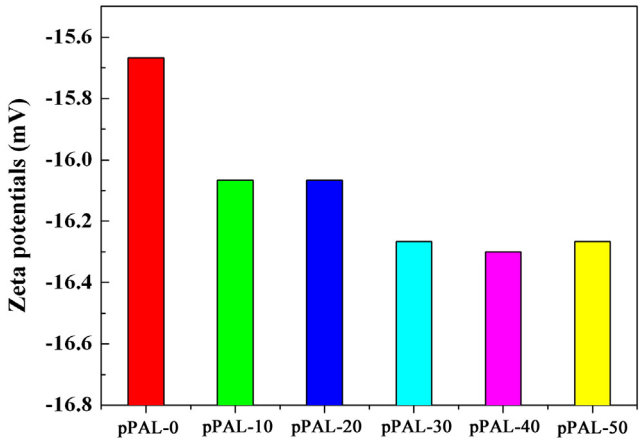

Fig. 4. Zeta potential of PAL modified under different homogenization pressures.

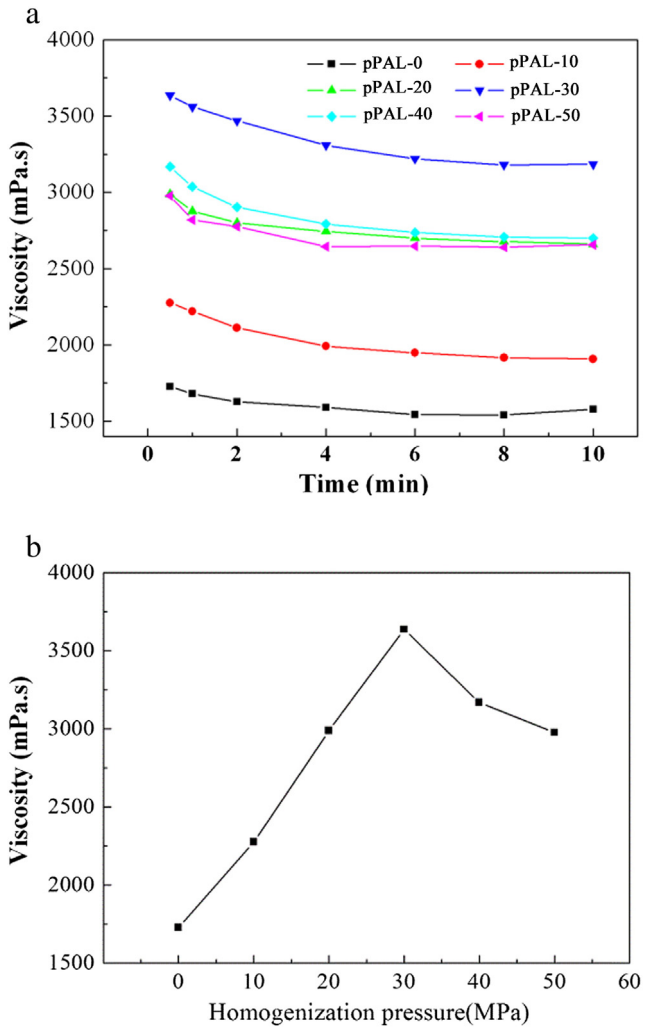

Fig. 5. Variation of viscosity of the PAL modified under different high-pressure homogenization pressures (a) and the viscosity of each sample at time 30 s (b).

More importantly, this process is simple, facile and suitable for large-scale industrial production.

The rotary viscosity of the PAL dispersion is closely related to the stability of the three-dimensional colloidal network composed of nanorods. The more stable is the network, the higher is the viscosity [16,21]. The main driving forces of forming the network structure are the "face-to-edge" electrostatic interaction between the positively charged "end" and the negatively charged "face" of PAL nanorod as well as the hydrogen bonding and van der Waals' force among surface groups. Thus, the viscosity is mainly dependent on the dispersion degree of nanorods, the aspect ratio of nanorod and the surface charge.

Before homogenization, the raw PAL existed as bulk crystal bundles or aggregates (Fig. 1a), which is difficult to form a stable colloidal network. With increasing the homogenization pressure, the dispersion degree of nanorods increased and the number of individual nanorods (the basic building units) gradually increased (Fig. 1). The dissociation of PAL crystal bundles into individual nanorods at moderate pressure is favorable to the self-assembly of nanorods and stability of gel network [21]. The improvement of network stability causes the increase of colloidal viscosity.

In addition, the surface potential of PAL was increased after modification with PA and HPH process, which may increase the association among nanorods and restrain the re-aggregation of the individually dispersed nanorods (Scheme 2). After being homogenized at 30 MPa, the dispersion degree of nanorods was clearly improved and more PA molecules attached on the surface of PAL. Thus, the surface charges and the dispersion of nanorods achieved an ideal balance point, and so the viscosity was sharply increased from 1728 mPa·s to 3636 mPa·s. With the further increase of homogenization pressure, some nanorods were broken and the aspect ratio of rods becomes smaller after treatment at too-high pressure. As a result, the intergranular coupling interaction becomes weak, and the viscosity of PAL dispersion exhibits a downward trend.

The colloidal stability was greatly improved after dispersion and modification. As shown in Fig. 6, all the samples almost reach the sedimentation equilibrium after settling for 48 h, and the dispersion of un-homogenized PAL sample was quickly decreased from 100 mL to 60.5 mL after settling for 12 h. However, the colloidal stability of PAL sample was greatly improved after homogenization treatment. The best colloidal stability of PAL dispersion was obtained after homogenization at 30 MPa. The dispersion of pPAL-30 can still maintain the interface level of 90 mL after settling for 108 h, which is closely related to the better dispersion as well as the relatively higher viscosity of the dispersion of pPAL-30 [24]. For the un-homogenized sample, it contains lots of crystal bundles and bulk particles or aggregates. The poor dispersion of PAL nanorods leads to the fast sedimentation of the dispersion. After homogenization at 30 MPa, the dispersibility of the PAL nanorods was improved and the sedimentation volume was increased, which indicate that the dissociation of crystal bundles, the surface charge and the viscosity of PAL dispersion have reached an ideal value after homogenization, which is favorable to improve the colloidal stability of the PAL dispersion.

3.3. Rheological properties

The flow curves of the PAL dispersion are shown in Fig. 7a. As can be seen, the shearing viscosity sharply decreased with increasing the shear rate, and the rheological curves show typical pseudoplastic flow behavior that is the main characteristic of clay minerals [40]. The modified PAL with PA molecules under high-pressure homogenization has relatively higher viscosity, which is consistent with the change tendency of rotary viscosity. As shown in Fig. 7b, the shear stresses increase with enhancing the homogenization pressure to 30 MPa (pPAL-30), and then slightly decreased with the further increase of pressure. The yield stress needed for the dispersion to start flowing was clearly observed. This implies that disaggregation of PAL crystal bundles may increase the association among nanorods in aqueous solution, and thus a stronger stress is required to break the connected clusters and orient the entangled rods in the flow direction.

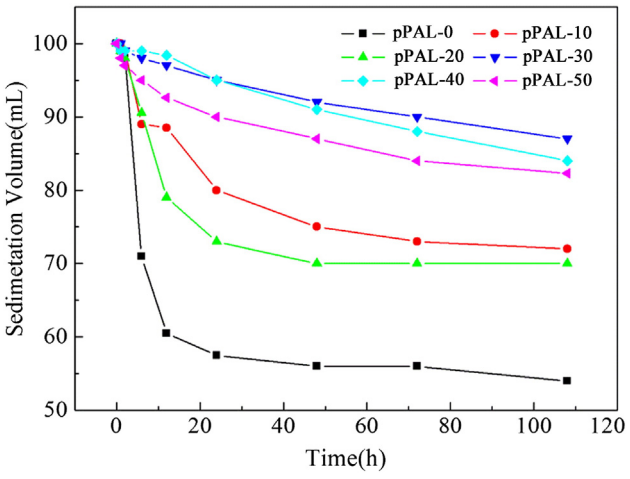

Fig. 6. The suspension property of the PAL modified under different homogenization pressures.

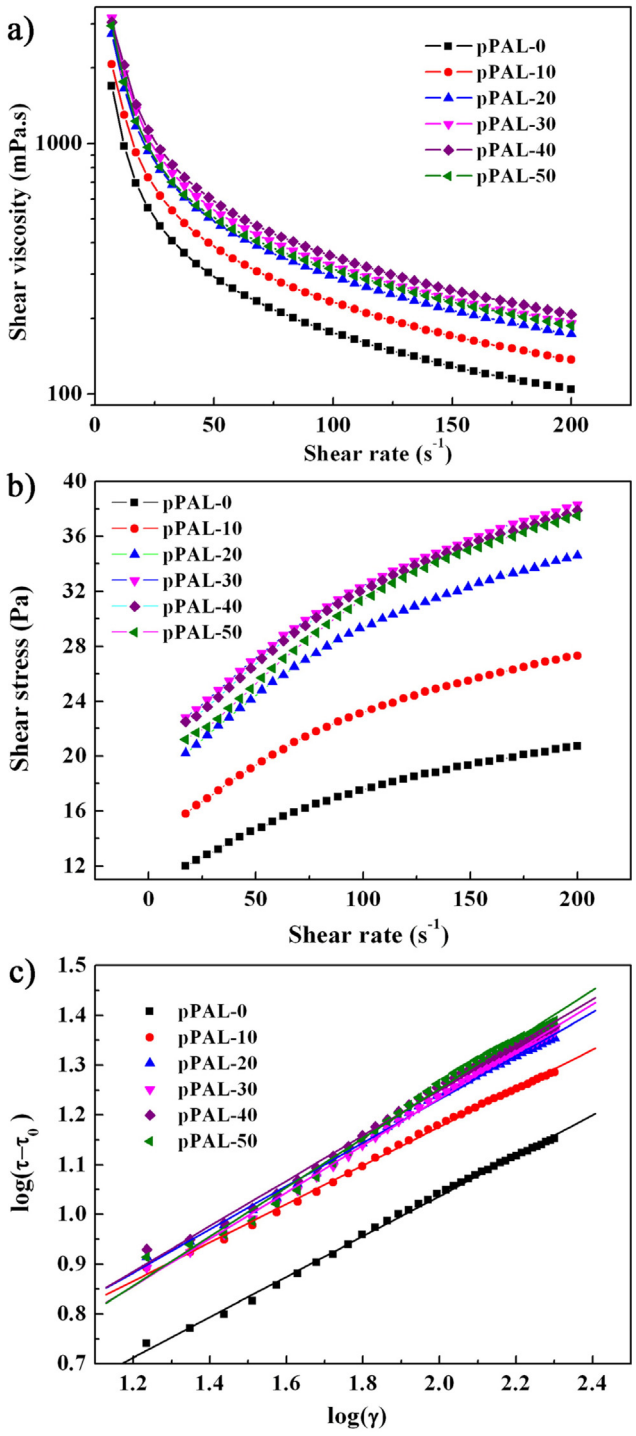

Fig. 7. (a) Shear rheological curves of PAL dispersion, (b) shear stress curves of PAL dispersion and (c) the fitting curves of log $(\tau - \tau_0)$ versus log (γ).

Pseudoplastic flow behavior of colloidal dispersion can be described by the Herschel–Bulkley (H–B) model [41]:

$$\tau = \tau_0 + m\gamma^a \quad (1)$$

where τ is the shear stress, τ_0 is the yield stress, γ is the shear rate, m is the consistency coefficient and a is the flow behavior index. Generally, the H–B model is used for the dispersion which has an initial yield stress at low shear rate, and afterwards presents a pseudoplastic or shear-thinning behavior at higher shear rate [42]. Therefore, the H–B model is suitable for fitting the rheological curves of PAL dispersion, and the fitting was carried out according to the method proposed by Coussot and Piau [43]. As shown in Fig. 7c, the plots of log $(\tau - \tau_0)$ versus log (γ) give straight lines with better linear correlation coefficients. The yield stress increases with increasing pressure, reached the maximum (15 Pa) at 30 MPa and then decreased. The yield stress of the modified PAL is always higher than the un-homogenized PAL. This indicates that nanoscale dispersion of PAL bundles by combining PA and HPH process is favorable to enhance the entanglement among rods more effectively.

The value of yield stress is a useful parameter to characterize the strength of inter-particle forces in a colloidal suspension. Some literature reported that yield stress is an indicator of the amount of stress required to reduce a flocculated system to a dispersion comprising only primary particles [44]. Like other clay systems, the colloidal properties of PAL dispersion are strongly correlated with the flocculation degree among the particles as well as the structure of flocs, and the rheological properties of PAL dispersion are quite sensitive to the dispersion state of the particle [45] and are not apparent until the bundles are being separated into individual rods [46]. Thus, the nanoscale dispersion of PAL crystal bundles is responsible for the increase of yield stress. As shown in Table 2, the resultant a values are smaller than 1, indicating that the suspension behaves not like Bingham fluid [47].

4. Conclusions

To improve the dispersion of rod-like crystal bundles or aggregates of PAL is significant to extend its application in modern industry, but there still lack simple, efficient and industrially available approaches to achieve the nanoscale dispersion of PAL rods. In this paper, the "physical" HPH technology and "chemical" PA-modification were combined to disperse PAL nanorods and improve its colloidal properties. The high-pressure homogenization process effectively dissociated the crystal bundles of PAL into individual nanorods without damaging the aspect ratio of PAL nanorods, and the simultaneous introduction of PA restrains the re-aggregation of dispersed nanorods. The nanoscale dispersion crystal bundles of PAL clearly enhanced the colloidal properties of PAL. The PAL modified with PA and homogenized at 30 MPa gives the best viscosity and stability. In contrast to the un-homogenized samples, the viscosity of PAL increased by 110.4% (from 1728 mPa·s to 3636 mPa·s), and the colloidal stability enhanced by 71%. The PA molecules only attach on the surface of PAL, and restrain the re-aggregation of nanorods by increasing the repulsion among rods.

The HPH technology has the rapid, high-efficient and safe advantages, and can be used for large-scale production of colloidal PAL product. The resulting product can be used as thicker, stabilizer, thixotropic agent, suspending agent and sizing agent, and shows great prospect in fine chemicals and petrochemical industry fields. The nanoscale dispersed PAL can be used as "aginomoto" (describes a filler that may cause greater improvement of performance by only adding a small dosage) of functional materials for high-end industrial applications.

Acknowledgment

The authors would like to thank "863" Project of the Ministry of Science and Technology of the People's Republic of China

Table 2
The yield stresses of PAL dispersion.

Samples	τ_0/Pa	a	R
pPAL-0	6.5	0.4061	0.9989
pPAL-10	8	0.3873	0.9990
pPAL-20	12	0.4360	0.9986
pPAL-30	15	0.4719	0.9988
pPAL-40	14	0.4559	0.9979
pPAL-50	13	0.4956	0.9961

(No. 2013AA032003), Natural Science Foundation of Gansu Provincial (No. 1208RJYA087) and the open funds of Key Laboratory for Palygorskite Science and Applied Technology of Jiangsu Province (No. HPK201201).

References

[1] S. Sinha Ray, M. Bousmina, Biodegradable polymers and their layered silicate nanocomposites: in greening the 21st century materials world, Prog. Mater. Sci. 50 (2005) 962–1079.
[2] B. Wang, G.X. Zhang, Z.M. Sun, S.L. Zheng, Synthesis of natural porous minerals supported TiO_2 nanoparticles and their photocatalytic performance towards Rhodamine B degradation, Powder Technol. 262 (2014) 1–8.
[3] J.W. Rhim, H.M. Park, C.S. Ha, Bio-nanocomposites for food packaging applications, Prog. Polym. Sci. 38 (2013) 1629–1652.
[4] W.F. Bradley, The structural scheme of attapulgite, Am. Mineral. 25 (1940) 405–410.
[5] E. Ruiz-Hitzky, M. Darder, F.M. Fernandes, B. Wicklein, A.C.S. Alcântara, P. Aranda, Fibrous clays based bionanocomposites, Prog. Polym. Sci. 38 (2013) 1392–1414.
[6] W.B. Wang, A.Q. Wang, Nanocomposite of carboxymethyl cellulose and attapulgite as a novel pH-sensitive superabsorbent: synthesis, characterization and properties, Carbohydr. Polym. 82 (2010) 83–91.
[7] Z.G. Qi, H.M. Ye, J. Xu, J.N. Chen, B.H. Guo, Improved the thermal and mechanical properties of poly(butylene succinate-*co*-butylene adipate) by forming nanocomposites with attapulgite, Colloids Surf. A Physicochem. Eng. Asp. 421 (2013) 109–117.
[8] D. Papoulis, S. Komarneni, D. Panagiotaras, P. Tsolis-Katagas, D. Panagiotaras, H.G. Kacandes, P. Zhang, S. Yin, T. Sato, H. Katsuki, Palygorskite–TiO_2 nanocomposites: part 1. Synthesis and characterization, Appl. Clay Sci. 83 (2013) 191–197.
[9] W.B. Wang, F.F. Wang, Y.R. Kang, A.Q. Wang, Facile self-assembly of Au nanoparticles on a magnetic attapulgite/Fe_3O_4 composite for fast catalytic decoloration of dye, RSC Adv. 3 (2013) 11515–11520.
[10] C.L. Huo, H.M. Yang, Preparation and enhanced photocatalytic activity of Pd–CuO/palygorskite nanocomposites, Appl. Clay Sci. 74 (2013) 87–94.
[11] E. Stathatos, D. Papoulis, C.A. Aggelopoulos, D. Panagiotaras, A. Nikolopoulou, TiO_2/palygorskite composite nanocrystalline films prepared by surfactant templating route: synergistic effect to the photocatalytic degradation of an azo-dye in water, J. Hazard. Mater. 211–212 (2012) 68–76.
[12] B. Sarkar, M. Megharaj, Y.F. Xia, R. Naidu, Surface charge characteristics of organo-palygorskites and adsorption of p-nitrophenol in flow-through reactor system, Chem. Eng. J. 185–186 (2012) 35–43.
[13] Y. Liu, Y.R. Kang, B. Mu, A.Q. Wang, Attapulgite/bentonite interactions for methylene blue adsorption characteristics from aqueous solution, Chem. Eng. J. 237 (2014) 403–410.
[14] A. Neaman, A. Singer, Rheological properties of aqueous suspensions of palygorskite, Soil Sci. Soc. Am. J. 64 (2000) 427–436.
[15] J.X. Xu, W.B. Wang, A.Q. Wang, M.S. Zheng, Dispersion of palygorskite in ethanol-water mixtures via high-pressure homogenization: microstructure and colloidal properties, Powder Technol 261 (2014) 98–104.
[16] D.E. Arnold, B.F. Bohor, H. Neff, G.M. Feinman, P.R. Williams, L. Dussubieux, R. Bishop, The first direct evidence of pre-Columbian sources of palygorskite for Maya Blue, J. Archaeol. Sci. 39 (2012) 2252–2260.
[17] L.H. Wang, J. Sheng, Preparation and properties of polypropylene/org-attapulgite nanocomposites, Polymer 46 (2005) 6243–6249.
[18] B. Xu, W.M. Huang, Y.T. Pei, Z.G. Chen, A. Kraft, R. Reuben, J.Th.M. De Hosson, Y.Q. Fu, Mechanical properties of attapulgite clay reinforced polyurethane shape-memory nanocomposites, Eur. Polym. J. 45 (2009) 1904–1911.
[19] D.J. Huang, W.B. Wang, J.X. Xu, A.Q. Wang, Mechanical and water resistance properties of chitosan/poly(vinyl alcohol) films reinforced with attapulgite dispersed by high-pressure homogenization, Chem. Eng. J. 210 (2012) 166–172.
[20] J. Zhou, N. Liu, Y. Li, Y.J. Ma, Microscopic structure characteristics of attapulgite, Bull. Chin. Ceram. Soc. (Chinese) 18 (1999) 50–55.
[21] J. Chen, Y. Jin, Y. Qian, T. Hu, A new approach to efficiently disperse aggregated palygorskite into single crystals via adding freeze process into traditional extrusion treatment, IEEE Trans. Nanotechnol. 9 (2010) 6–10.
[22] J.X. Xu, W.B. Wang, A.Q. Wang, Influence of anions on the electrokinetic and colloidal properties of palygorskite clay via high-pressure homogenization, J. Chem. Eng. Data 58 (2013) 764–772.
[23] S. Schultz, G. Wagner, K. Urban, J. Ulrich, High-pressure homogenization as a process for emulsion formation, Chem. Eng. Technol. 27 (2004) 361–368.
[24] J.X. Xu, J.P. Zhang, A.Q. Wang, Disaggregation of palygorskite crystal bundles via high-pressure homogenization, Appl. Clay Sci. 54 (2011) 118–123.
[25] J.X. Xu, A.Q. Wang, Electrokinetic and colloidal properties of homogenized and unhomogenized palygorskite in the presence of electrolytes, J. Chem. Eng. Data 57 (2012) 1586–1593.
[26] E. Graf, K.L. Empson, J.W. Eaton, Phytic acid. A natural antioxidant, J. Biol. Chem. 262 (1987) 11647–11650.
[27] K. Dost, O. Tokul, Determination of phytic acid in wheat and wheat products by reverse phase high performance liquid chromatography, Anal. Chim. Acta. 558 (2006) 22–27.
[28] K. Wang, P.C. Liu, Y.H. Ye, J. Li, W.B. Zhao, X.H. Huang, Fabrication of a novel laccase biosensor based on silica nanoparticles modified with phytic acid for sensitive detection of dopamine, Sensors Actuators B 197 (2014) 292–299.
[29] J.E. Chisholm, Powder-diffraction patterns and structural models for palygorskite, Can. Mineral. 30 (1992) 61–73.
[30] J.E. Post, P.J. Heaney, Synchrotron powder X-ray diffraction study of the structure and dehydration behavior of palygorskite, Am. Mineral. 93 (2008) 667–675.
[31] Z. Darvishi, A. Morsali, Sonochemical preparation of palygorskite nanoparticles, Appl. Clay Sci. 51 (2011) 51–53.
[32] L. Boudriche, A. Chamayou, R. Calvet, B. Hamdi, H. Balard, Influence of different dry milling processes on the properties of an attapulgite clay, contribution of inverse gas chromatography, Powder Technol. 254 (2014) 352–363.
[33] R.L. Frost, O.B. Locos, H. Ruan, J.T. Kloprogge, Near-infrared and mid-infrared spectroscopic study of sepiolites and palygorskites, Vib. Spectrosc. 27 (2001) 1–13.
[34] M. Suárez, E. García-Romero, FTIR spectroscopic study of palygorskite: influence of the composition of the octahedral sheet, Appl. Clay Sci. 31 (2006) 154–163.
[35] W. Kuang, G.A. Facey, C. Detellier, Dehydration and rehydration of palygorskite and the influence of water on the nanopores, Clay Clay Miner. 52 (2004) 635–642.
[36] J.X. Xu, W.B. Wang, A.Q. Wang, Effects of solvent treatment and high-pressure homogenization process on dispersion properties of palygorskite, Powder Technol. 235 (2013) 652–660.
[37] S.H. Lin, R.S. Juang, Heavy metal removal from water by sorption using surfactant-modified montmorillonite, J. Hazard. Mater. 92 (2002) 315–326.
[38] National Standard of the People's Republic of China, GB6900.11-86. Fireclay and high-alumina refractories—determination of phosphorus pentoxide content—molybdenum blue photometric method.
[39] M. Alkan, Ö. Demirbaş, M. Doğan, Electrokinetic properties of sepiolite suspensions in different electrolyte media, J. Colloid Interface Sci. 281 (2005) 240–248.
[40] H. Van Olphen, An Introduction to Clay Colloid Chemistry, second ed. John Wiley & Sons, New York, 1977.
[41] W. Herschel, R. Bulkley, Konsistenzmessungen von Gummi-Benzollösungen, Colloid Polym. Sci. 39 (1926) 291–300.
[42] P.F. Luckham, S. Rossi, The colloidal and rheological properties of bentonite suspensions, Adv. Colloid Interf. Sci. 82 (1999) 43–92.
[43] P. Coussot, J.M. Piau, On the behavior of fine mud suspensions, Rheol. Acta 33 (1994) 175–184.
[44] A.E. James, D.J.A. Williams, Particle interactions and rheological effects in kaolinite dispersions, Adv. Colloid Interf. Sci. 17 (1982) 219–232.
[45] J.H. Xu, S. Chatterjee, K.W. Koelling, Y.R. Wang, S.E. Bechtel, Shear and extensional rheology of carbon nanofiber suspensions, Rheol. Acta 44 (2005) 537–562.
[46] W.L. Haden Jr., Palygorskite: properties and uses, Clay Clay Miner. (1963) 284–290.
[47] B. Abu-Jdayil, Rheology of sodium and calcium bentonite–water dispersions: effect of electrolytes and aging time, Int. J. Miner. Process 98 (2011) 208–213.